Applied Catalysis B: Environmental 111–112 (2012) 409–414

Contents lists available at SciVerse ScienceDirect

Applied Catalysis B: Environmental

journal homepage: www.elsevier.com/locate/apcatb

Red phosphorus: An elemental photocatalyst for hydrogen formation from water

Feng Wang[a], Wilson Kwok Hung Ng[b], Jimmy C. Yu[a,*], Haojun Zhu[c], Chuanhao Li[a], Lei Zhang[a], Zhifeng Liu[b], Quan Li[c]

[a] Department of Chemistry and Institute of Environment, Energy and Sustainability, The Chinese University of Hong Kong, Shatin, New Territories, Hong Kong, China
[b] Department of Chemistry and Centre for Scientific Modeling and Computation, The Chinese University of Hong Kong, Shatin, New Territories, Hong Kong, China
[c] Department of Physics, The Chinese University of Hong Kong, Shatin, New Territory, Hong Kong, China

ARTICLE INFO

Article history:
Received 28 August 2011
Received in revised form 18 October 2011
Accepted 18 October 2011
Available online 25 October 2011

Keywords:
Elemental photocatalyst
Hydrogen formation
Red phosphorus
Semiconductor

ABSTRACT

A novel property of red phosphorus for visible light driven photocatalytic H_2 formation from water by photogenerated electrons has been discovered. The detection of hydroxyl radicals and results from photoconductivity measurements confirmed the photogeneration of electrons and holes. Theoretical calculations also indicated that the reduction of water by photogenerated electrons would be energetically possible. A P-type semiconductor behavior of red phosphorus was observed. Our findings may provide insights for developing phosphorus-based photocatalysts.

1. Introduction

The finding of new properties of materials, especially for elemental materials, has ignited revolutions in science and technology. Over the past decade, new applications have been discovered for silicon and carbon materials in optical, electronical, optoelectronical and photocatalytical research fields [1–4]. Photocatalytic hydrogen production from water is a clean and renewable source of energy [5–9]. In this system, a photocatalyst with a suitable conduction band energy for transferring the photogenerated electrons to water is needed [10]. Moreover, the band gap of a desirable photocatalyst should be around 2.0 eV to utilize solar energy effectively. Because of these stringent requirements, it is difficult to develop new visible-light-driven photocatalysts, especially simple elemental ones. For example, silicon quantum dots have been employed as a photocatalyst for the degradation of methyl red and the oxidization of benzene [11]. However, this element cannot be used alone in water splitting due to its unsuitable bandgap structure [12]. Recently, a complicated system of poly(ethylene glycol) diamine functionalized carbon nanoparticles with gold or platinum coating was found to be somewhat active for hydrogen evolution from water [13]. Much simpler materials must be used for photocatalytic systems to be economically viable. This communication reports for the first time the novel photocatalytic property of elemental red phosphorus.

Red phosphorus is one of the most versatile elements. It is used in organic chemistry and chemical warfare, including igniters, incendiaries, screening smoke ammunition and smoke signal [14–16]. Recently, phosphorus was incorporated into titanium dioxide to improve the solar spectrum response of TiO_2 [17,18]. This band gap narrowing is probably due to the mixing of the P 3p and O 2p states [19]. Pure red phosphorus by itself as a solar-responsive photocatalyst, however, has never been reported. Photocatalytic systems based on elemental substances are obviously a more elegant approach than those involving highly complex materials.

2. Experimental

2.1. Preparation of crystalline red phosphorus

Commercial red phosphorus was dispersed in water and put into a Teflon-lined stainless autoclave. The autoclave was heated to 200 °C and maintained for 12 h to remove surface oxidation. The treated red phosphorus was crystallized in a vacuum tube furnace at 450 °C for 12 h. The crystallized product was washed with water and methanol, and then dried at 60 °C. Different amounts of Pt loaded red phosphorus were prepared by photochemical reduction of H_2PtCl_6 in presence of red phosphorus aqueous suspension.

2.2. Preparation of red phosphorus films

Red phosphorus films were prepared by a vacuum deposition method. 100 mg of red phosphorus powder were put into a quartz glass tube (0.7 cm × 5.0 cm) with a quartz sheet (0.5 cm × 2.0 cm)

* Corresponding author. Tel.: +852 3943 6268; fax: +852 2603 5057.
E-mail address: jimyu@cuhk.edu.hk (J.C. Yu).

0926-3373/$ – see front matter © 2011 Elsevier B.V. All rights reserved.
doi:10.1016/j.apcatb.2011.10.028

inside. The system was sealed under vacuum. The glass tube was heated to 650 °C at 1 °C min^{-1} and kept at that temperature for 12 h. The resulting sheets were cut into the size of 0.5 cm × 0.5 cm for photoconductivity measurements and electrical tests. The film thickness was ca. 10 μm as measured by a Techcor Alpha-Step 500 Surface Profilter system.

2.3. Characterizations

Scanning electron microscopy (SEM) imaging was recorded on a FEI Quanta 400 microscope. Standard transmission electron microscopy (TEM) images were recorded using a CM-120 microscope (Philips, 120 kV) coupled with an energy-dispersive X-ray (EDX) spectrometer (Oxford Instrument). The electron microscopy samples were prepared by dispersing the powder in ethanol with ultrasonication for 20 s. XRD patterns were recorded with a Rigaku SmartLab X-ray diffractometer using Cu Kα irradiation (λ = 1.5406 Å). The accelerating voltage and applied current were 40 kV and 40 mA. The BET surface areas were measured by a Micromertics ASAP 2010 instrument. UV–vis diffuse reflectance spectra were achieved using a UV–vis spectrophotometer (Cary 100 scan spectrophotometers, Varian). The concentration of phosphate ions leaching from the possible dissolution of red phosphorus were measured by Metrohm 792 Basic Ion Chromatography with a column of Grace Allsep Anion 7u (150 mm × 4.6 mm). The eluent was 2.0 mM $NaHCO_3$ and 0.8 mM Na_2CO_3.

2.4. Gas evolution tests

The photocatalytic H_2 evolution experiments were carried out in a Pyrex reaction cell connected to a closed gas circulation and evacuation system. 50 mg of the sample were dispersed in 100 mL of aqueous solution containing 5 vol% methanol as a hole sacrificial agent. The suspension was purged with argon to remove dissolved air before irradiation. The solution was irradiated by a 300 W xenon lamp with an appropriate cut-off filter and a water filter (a 400 nm cut-off filter was used in all tests except the experiment related to Fig. 7b). The amount of hydrogen generated from photocatalytic water splitting was measured by Techcomp GC7900 gas chromatography with TCD detector and a capillary column (molecular sieve 5 Å). High purity nitrogen gas was used as a carrier gas. A control experiment was carried out without the addition of methanol. Amounts of O_2 were measured under the same condition with that of H_2 except high purity helium gas was used as a carrier gas.

2.5. Detection of photogenerated OH radicals

A stock terephthalic acid solution with final concentrations of 4×10^{-4} M terephthalic acid and 2×10^{-3} M NaOH was prepared. 30 mg of crystalline P were added to 40 mL of the stock solution. The suspension was irradiated by a 300 W halogen lamp (with a 400 nm filter). At every 30 min, 2 mL of the suspensions were collected and centrifugated. The resulted supernatants were diluted four times for PL measurements. Fluorescence spectra of generated 2-hydroxyterephthalic acid were measured on a Hitachi F-4500 fluorescence spectrophotometer with an excitation wavelength of 320 nm.

2.6. Computational details

VASP computational package was used for all the calculations in this article [20–23]. We applied projector-augmented-wave method with Perdew–Burke–Ernzerhof GGA functional [24–26]. Electronic convergence limit was set to be 1×10^{-5} eV. Optimization of atomic coordinates was considered to be converged if Hellmann–Feynman force was smaller than 1×10^{-2} eV Å^{-1}. The slab consists of 4-layers of polyphosphide tubes exposing (0 0 1) and (0 0 $\bar{1}$) surface. The 2 polyphosphide tubes layers in the middle were held fixed during optimization. The vacuum region is about 12 Å in height. We applied Monkhorst–Pack scheme 3 × 3 × 1 for *k*-point selection and resulted in 5 irreducible *k*-points.

2.7. Photoconductivity measurements and electrical tests

Two Ag wires were connected to the opposite edges of the film by using Ag conductive epoxy. Photoconductivity measurements were carried out on an electrochemical workstation (CHI 660C, Shanghai Chen Hua Instrument Company, China). Photocurrent–voltage and the photocurrent response to on–off cycles were recorded under the illumination of a fiber optics equipped with a tungsten lamp (Cole-Parmer illuminator, 41720 series). The light intensity was about 200 mW/cm^2.

Electrical properties of the red phosphorus films were measured by the Van der Pauw 4-probe method (Bio-Rad Hall System) [27]. The mobility was calculated from the sheet resistance and Hall coefficient.

3. Experimental results and discussion

3.1. Sample characterizations

The crystalline red phosphorus was synthesized by heating an amorphous red phosphorus under vacuum at 450 °C (see Section 2) [28]. Fig. 1a and b shows the morphology of crystalline red phosphorus, indicating the product is microparticles with a layer of nanorods on their surface. The selected-area electron diffraction (SAED) pattern reveals the single-crystal nature of nanorods (Fig. 1d). Fig. 1c shows a typical XRD pattern of the product. All the diffraction peaks are readily indexed to the standard monoclinic phase of phosphorus (JCPDS card no. 44-0906). The absorption edge of red phosphorus shifts from 700 nm to 680 nm after crystallization, as shown in Fig. 2. The blue-shift is due to decreased imperfections and disordering of structure [29]. The bandgap of crystalline red phosphorus is estimated to be 1.7 eV.

3.2. Photocatalytic H_2 formation over red phosphorus

Rates for H_2 evolution were measured by irradiating a 100 mL of solution containing 50 mg of products and 5 mL of methanol (as a hole sacrificial agent). H_2 is produced at a rate of 0.08 μmol h^{-1} for crystalline red phosphorus. An amorphous red phosphorus sample is also tested and found to be only half as effective for hydrogen evolution (Fig. 2). As the BET surface area of the crystalline red phosphorus (ca. 39 m^2/g) is larger than that of amorphous one (ca. 18 m^2/g), the enhanced photocatalytic activity after crystallization can be explained by the increased surface area and a decrease in the number of electron–hole trapping centers [30,31]. The gas evolution stopped when the light was turned off, suggesting the reaction was initiated by the absorption of visible light. It is noted that a small amount of oxygen was detected on crystalline red phosphorus samples (data not shown), indicating the presence of a trace amount of P_2O_5. P_2O_5 is a white powder and control experiments show no photocatalytic activity over it. Our results clearly indicate that red phosphorus exhibits a photocatalytic property for H_2 formation from water under irradiation.

Different amounts of platinum was loaded onto red phosphorus by photo-reduction of a H_2PtCl_6 solution to investigate their photocatalytic performance. The mean diameter of the loaded Pt NPs is ca. 12 nm and the range is from 5 nm to 20 nm (Fig. S1). The rate constants were calculated from Fig. S2, and are summarized in

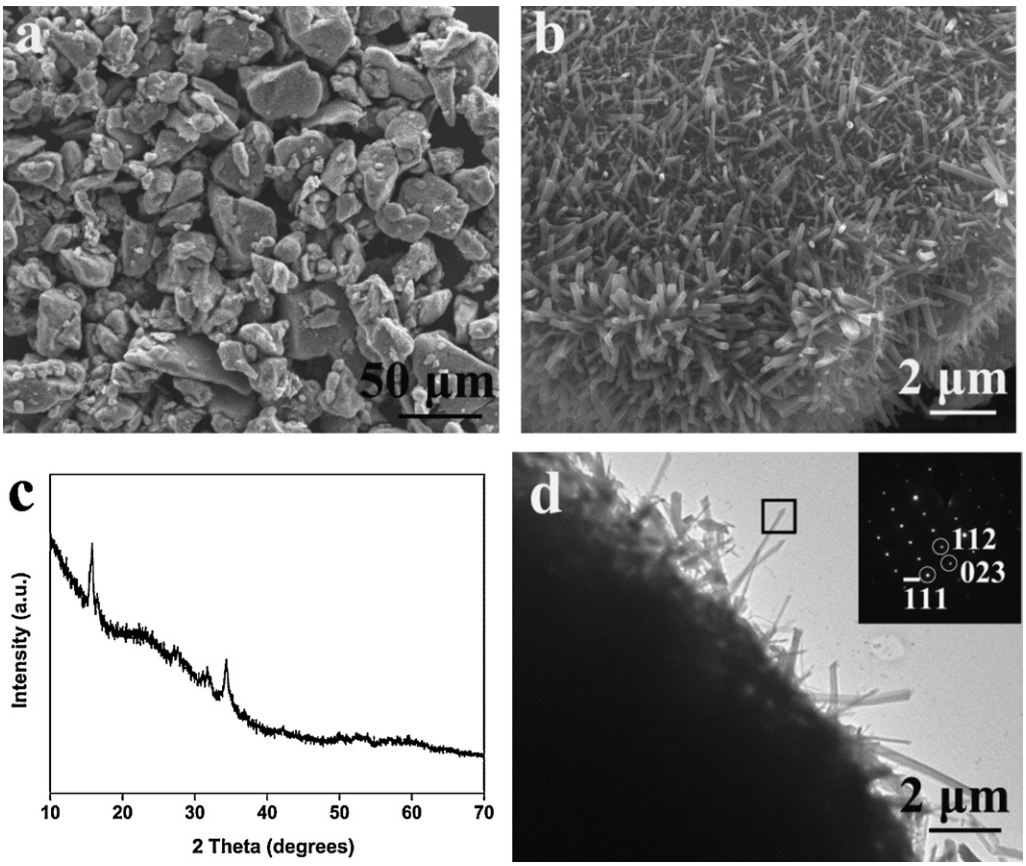

Fig. 1. (a and b) SEM images, (c) a typical XRD pattern and (d) TEM image (inset is ED patterns of marked square region) of crystalline red phosphorus.

Table S1. Results show that the H_2 production rate is increased with increasing Pt content to a plateau at around 1–3 wt%, beyond which it decreases again. The activity of red phosphorus is increased by over 10 times with the addition of 1 wt% of Pt. These results could be explained by a small amount of Pt (1–3 wt%) act as an effective cocatalyst by lowing the activation potential of H_2 formation and suppressing the recombination of photogenerated charges. However, excess amounts of cocatalyst (4 wt% or higher) would increase the number of electron–hole recombination centers, resulting in a lower efficiency [32,33].

To evaluate the stability of the photocatalyst, reactions were allowed to proceed for 90 h with intermittent evacuation at 30 h intervals. Fig. 3a shows a virtually constant rate for H_2 evolution over the duration of reactions under visible light irradiation. The same high stability is observed even under full spectral irradiation from a 300 W xenon lamp (Fig. 3b). The XRD pattern indicates that the monoclinic phase of red phosphorus is well maintained after the reaction (data not shown).

To confirm the water photolysis process, we conducted a control experiment in the absence of methanol. H_2 and O_2 are steadily produced under irradiation. The molar ratio of H_2/O_2 is nearly 2/1 (Fig. 4). These results confirm that H_2 comes from photoreduction of water. As expected, the rate of H_2 formation decreases by about 4 times in the absence of methanol, suggesting methanol functions as a sacrificial agent to consume the photogenerated holes and improve the efficiency of red phosphorus [30].

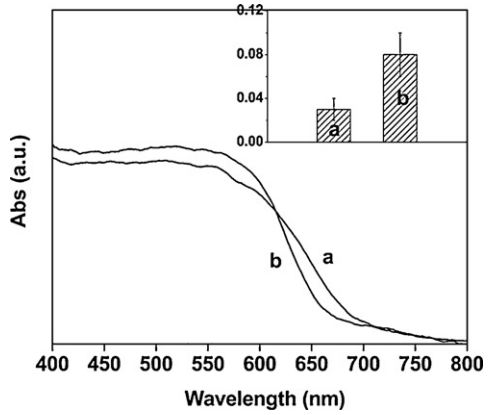

Fig. 2. UV–visible diffuse reflectance spectra of (a) amorphous and (b) crystalline red phosphorus. Insert figure shows rates of H_2 formation over (a) amorphous and (b) crystalline red phosphorus. Reaction conditions: 50 mg of photocatalyst, 95 mL of water, 5 mL of methanol and a 300 W xenon lamp.

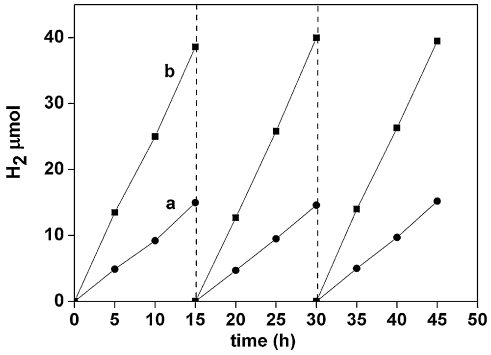

Fig. 3. A typical time course of H_2 production from aqueous methanol solution by 1 wt% Pt loaded crystalline red phosphorus under (a) the visible light and (b) the full spectrum of xenon lamp irradiation. Reaction conditions: 50 mg of photocatalyst, 95 mL of water, 5 mL of methanol and a 300 W xenon lamp.

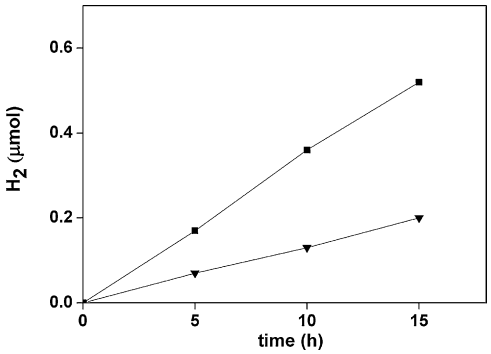

Fig. 4. Time courses of H_2 and O_2 production from pure water over crystalline red phosphorus under visible light irradiation. Reaction conditions: 50 mg of photocatalyst, 100 mL of water and a 300 W xenon lamp with a 400 nm filter.

3.3. Stability of red phosphorus

To determine if red phosphorus would be oxidized under irradiation, the concentration of phosphate ions were measured during the reaction. Ion chromatography was used to analyze the reaction solution which was irradiated by the xenon lamp. Trace levels of phosphate and hydrogen phosphate ions are detected (Fig. 5). The concentrations of PO_4^{3-} and HPO_4^{2-} increase in the first 12 h, and then are kept almost constant at 26.4 and 48.5 ppm, respectively from one to three days of irradiation.

3.4. Detection of photogenerated OH radicals

To verify that hydrogen came from photocatalytic reduction of water, a photoluminescence method was employed to detect hydroxyl radicals with terephthalic acid as the probe molecule [34,35]. As shown in Fig. 6a, terephthalic acid captures hydroxyl radicals to produce a highly fluorescent 2-hydroxyterephthalic acid which emits at 440 nm upon UV excitation. The increasing fluorescence intensities confirm the involvement of hydroxyl radicals in the photocatalytic pathway (Fig. 6b).

3.5. Photoconductivity measurements and electrical tests

Fig. 7a shows photocurrent–voltage plots of a red phosphorus film under both dark and illumination conditions. The resistance of the film is significantly decreased under illumination (200 MΩ/cm^2) than in the dark (6.7 MΩ/cm^2). Fig. 7b shows the photocurrent response of red phosphorus film to on–off cycles of illumination at about 1 s intervals with a bias potential of 1.0 V. The photocurrent is 0.09 μA/cm^2 after light on and drops

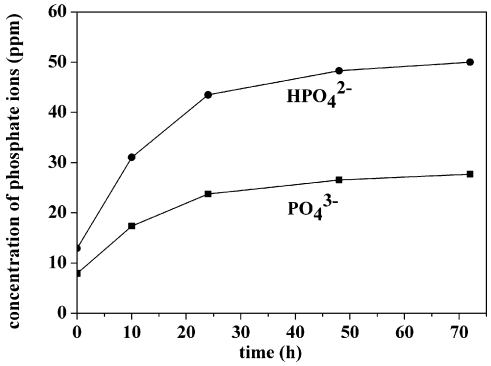

Fig. 5. The concentration of phosphate and hydrogen phosphate ions *vs* irradiation time during H_2 evolution by using 50 mg of red phosphorus under 300 W xenon lamp irradiation.

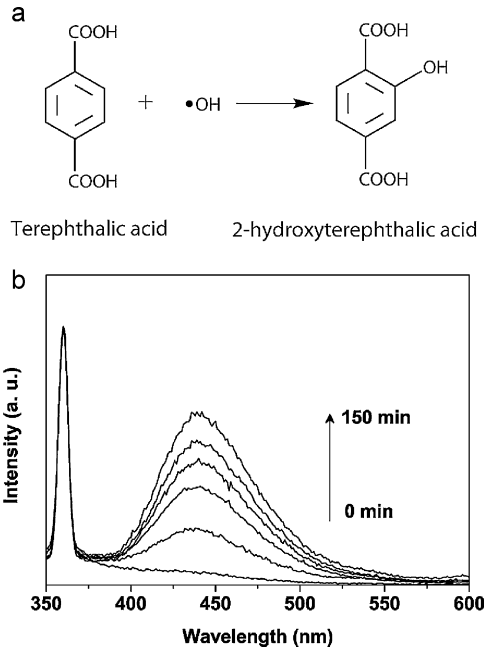

Fig. 6. (a) Reaction between the formed OH radicals and terephthalic acid. (b) Time-dependent fluorescence spectra of the terephthalic acid solution (4×10^{-4} M). Each fluorescence spectrum was recorded every 30 min of visible light illumination.

to 0.002 μA/cm^2 without illumination. These results verify that electrons and holes are generated over red phosphorus under illumination.

The Van der Pauw 4-probe method was used to determine whether the red phosphorus film was a P-type or N-type semiconductor. A mobility of 8.05 cm^2/V s was obtained indicating that red phosphorus should be considered a P-type semiconductor.

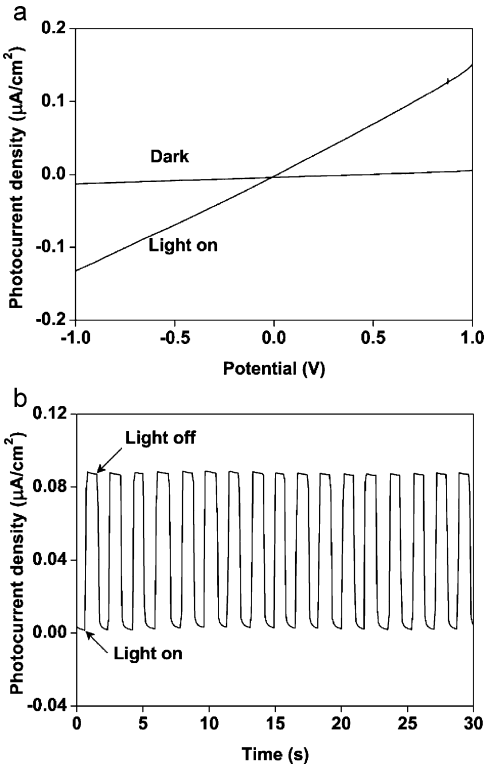

Fig. 7. (a) Photocurrent–voltage curves of red phosphorus film under dark and illumination conditions. (b) Photocurrent response of red phosphorus film to on–off cycles of illumination at about 1 s intervals with a bias potential of 1.0 V.

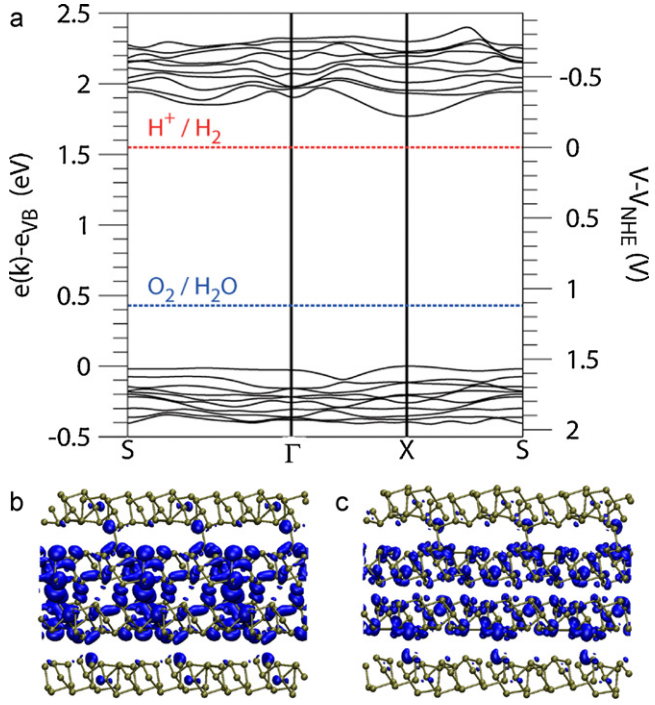

Fig. 8. (a) The figure shows the DFT band structure for red phosphorous slab with (0 0 1) and (0 0 $\bar{1}$) surface exposed. *X* and *S* represent (0.5 0.0 0.0) and (0.5 0.5 0) *k*-point in reciprocal space. The position for reduction level of H^+ to H_2 and oxidation level of H_2O to O_2 are marked with color lines. Band decomposed charge density for (b) highest valence band and (c) lowest conduction band were shown and the isosurface charge density was chosen to be 0.005 q_e Å^{-3} for display.

3.6. Theoretically evaluation

To elucidate the reduction ability of the photogenerated electrons from red phosphorus, the band structures were calculated. The coordination data of Hittorf's phosphorous were used for computation and we re-optimized the unit cell including both the lattice constants and the coordinates of phosphorous atoms [36]. Fig. 8 shows the band structure of slab exposing (0 0 1) and (0 0 $\bar{1}$) surface and the charge density isosurfaces of highest valence band and lowest conduction band. The calculated band gap is ca. 1.8 eV. It is in agreement with the experimental result. The reduction level of hydrogen $\mu_e{}^{H^+/H_2} = -4.18$ eV lies within the band gap [31]. These results suggest reduction of water by red phosphorus under irradiation is energetically possible.

3.7. Proposed mechanism

The mechanism of red phosphorus for photocatalytic H_2 formation over water was proposed as Scheme 1. Under irradiation, red phosphorus could be excited with the formation of photogenerated electrons and holes (corresponding Formula (a)). The holes would be consumed by methanol (Formula (b)) and the electrons were immigrated onto Pt surface. Then, H_2 was formed by reducing H_2O on the surface of Pt particles (Formula (c)).

$$\mathrm{RedP} + h\upsilon \rightarrow \mathrm{h^+(P)} + \mathrm{e^-(P)} \quad \text{(a)}$$

$$\mathrm{h^+} + \mathrm{CH_3OH} \rightarrow \mathrm{HCOOH/HCHO} \quad \text{(b)}$$

$$\mathrm{e^-} + \mathrm{H_2O} \xrightarrow{\mathrm{Pt}} \mathrm{H_2} + \mathrm{OH^-} \quad \text{(c)}$$

Compared with the reported visibile-light-driven photocatalysts, red phosphorus has advantages of simplicity and wide-spectral adsorption of solar light. Moreover, red phosphorus can be easily modified with metal phosphide or phosphate by the reaction with metal salts for developing efficient heterophotocatalysts [37].

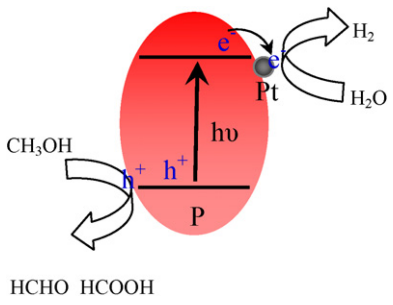

Scheme 1. The proposed mechanism for photocatalytic H_2 formation over red phosphorus.

4. Conclusions

In summary, we discovered a new semiconductor property of red phosphorus for photocatalytic hydrogen evolution from water under visible light irradiation. The activity could be increased by 12 times after loading 1 wt% Pt as a cocatalyst. A mechanism for H_2 formation by reducing water with photogenerated electrons was proposed. The detection of hydroxyl radicals and results from photoconductivity measurements confirmed the photogeneration of electrons and holes. Theoretical calculations indicated the strong reduction capacity of photogenerated electrons. Results from Van der Pauw 4-probe tests suggested a P-type semiconductor behavior for red phosphorus. Our findings may provide insights for developing phosphorus-based photocatalysts for hydrogen production from water. It also would be beneficial for understanding of physical properties of red phosphorus and discovering interesting applications.

Acknowledgements

Mingdong Wang and Prof. Jianbin Xu of the Department of Electronic Engineering are gratefully acknowledged for their help in electrical tests and valuable discussions. The work described in this paper was partially supported by the Focused Investment Scheme of The Chinese University of Hong Kong and a grant from the Research Grants Council of the Hong Kong Special Administration Region, China (Project 404810).

Appendix A. Supplementary data

Supplementary data associated with this article can be found, in the online version, at doi:10.1016/j.apcatb.2011.10.028.

References

[1] B. Tian, T.J. Kempa, C.M. Lieber, Chem. Soc. Rev. 38 (2009) 16–24.
[2] C.K. Chan, H.L. Peng, G. Liu, K. McIlwrath, X.F. Zhang, R.A. Huggins, Y. Cui, Nat. Nanotechnol. 3 (2008) 31–35.
[3] K.S. Novoselov, A.K. Geim, S.V. Morozov, D. Jiang, Y. Zhang, S.V. Dubonos, I.V. Grigorieva, A.A. Firsov, Science 306 (2004) 666–669.
[4] C.N.R. Rao, A.K. Sood, K.S. Subrahmanyam, A. Govindaraj, Angew. Chem. Int. Ed. 48 (2009) 7752–7777.
[5] A. Fujishima, K. Honda, Nature 238 (1972) 37–38.
[6] F.E. Osterloh, Chem. Mater. 20 (2008) 35–54.
[7] X.L. Hu, G.S. Li, J.C. Yu, Langmuir 26 (2010) 3031–3039.
[8] Z.G. Zou, J.H. Ye, K. Sayama, H. Arakawa, Nature 414 (2001) 625–627.
[9] W.F. Yao, C.P. Huang, N. Muradov, A. T-Raissi, Int. J. Hydrogen Energy 36 (2011) 4710–4715.
[10] K. Maeda, K. Domen, Photocatalytic J. Phys. Chem. Lett. 265 (2010) 2655–2661.
[11] Z.H. Kang, C.H.A. Tsang, N.B. Wong, Z.D. Zhang, S.T. Lee, J. Am. Chem. Soc. 129 (2007) 12090–12091.
[12] R.Q. Zhang, X.M. Liu, Z. Wen, Q. Jiang, J. Phys. Chem. C 115 (2011) 3425–3428.

[13] L. Cao, S. Sahu, P. Anilkumar, C.E. Bunker, J. Xu, K.A.S. Fernando, P. Wang, E.A. Guliants, I. Tackett, K.N.Y.P. Sun, J. Am. Chem. Soc. 133 (2011) 4754–4757.
[14] B.A. Trofimov, N.K. Gusarova, Mendeleev Commun. 19 (2009) 295–302.
[15] M. Scheer, G. Balázs, A. Seitz, Chem. Rev. 110 (2010) 4236–4256.
[16] E.C. Koch, Propell. Explos. Pyrot. 33 (2008) 165–176.
[17] C.L. Yu, J.C. Yu, W.Q. Zhou, K. Yang, Catal. Lett. 140 (2010) 172–183.
[18] N. Comsup, J. Panpranot, P. Praserthdam, Catal. Commun. 11 (2010) 1238–1243.
[19] R.Y. Zheng, Y. Guo, C. Jin, J.L. Xie, Y.X. Zhu, Y.C. Xie, J. Mol. Catal. A: Chem. 319 (2010) 46–51.
[20] G. Kresse, J. Hafner, Phys. Rev. B 47 (1993) 558–561.
[21] G. Kresse, J. Hafner, Phys. Rev. B 49 (1994) 14251–14269.
[22] G. Kresse, J. Furthmuller, Comput. Mater. Sci. 6 (1996) 15–50.
[23] G. Kresse, J. Furthmuller, Phys. Rev. B 54 (1996) 11169–11186.
[24] P.E. Blochl, Phys. Rev. B 50 (1994) 17953–17979.
[25] G. Kresse, D. Joubert, Phys. Rev. B 59 (1999) 1758–1775.
[26] J.P. Perdew, K. Burke, M. Ernzerhof, Phys. Rev. Lett. 77 (1996) 3865–3868.
[27] L.J. Van der Pauw, Philips Tech. Rev. 59 (1958) 220–224.
[28] W.L. Roth, T.W. DeWitt, A.J. Smith, J. Am. Chem. Soc. 69 (1947) 2881–2885.
[29] R. Elilarassi, G. Chandrasekaran, Mater. Chem. Phys. 121 (2010) 378–384.
[30] X.B. Chen, S.H. Shen, L.J. Guo, S.S. Mao, Chem. Rev. 110 (2010) 6503–6570.
[31] X.C. Wang, K. Maeda, A. Thomas, K. Takanabe, G. Xin, J.M. Carlsson, K. Domen, M. Antonietti, Nat. Mater. 8 (2009) 76–80.
[32] B.J. Ma, F.Y. Wen, H.F. Jiang, J.H. Yang, P.L. Ying, C. Li, Catal. Lett. 134 (2010) 78–86.
[33] B. Kraeutler, A.J. Bard, J. Am. Chem. Soc. 100 (1978) 4317–4318.
[34] K. Ishibashi, A. Fujishima, T. Watanabe, K. Hashimoto, Electrochem. Commun. 2 (2000) 207–210.
[35] C.H. Li, F. Wang, J. Zhu, J.C. Yu, Appl. Catal. B: Environ. 100 (2010) 433–439.
[36] V.H. Thurn, H. Krebs, Acta Cryst. B25 (1969) 125–135.
[37] B.M. Barry, E.G. Gillan, Chem. Mater. 20 (2008) 2618–2620.